Magneto-electronic interactions in $La_{0.8}Ca_{0.2}MnO_3$ perovskite

1999 J. Phys.: Condens. Matter 11 8901

(http://iopscience.iop.org/0953-8984/11/45/313)

J. Phys.: Condens. Matter **11** (1999) 8901–8912. Printed in the UK PII: S0953-8984(99)06379-1

Magneto-electronic interactions in $La_{0.8}Ca_{0.2}MnO_3$ perovskite

F Walz, J H V J Brabers and H Kronmüller

Max-Planck-Institut für Metallforschung, Heisenbergstrasse 1, D-70569 Stuttgart, Germany

Received 27 July 1999

Abstract. By means of extended magnetic after-effect (MAE) and electric resistivity measurements (4 K $< T <$ 300 K), polycrystalline $La_{0.8}Ca_{0.2}MnO_3$ has been identified below the Curie temperature ($T_C \simeq$ 190 K), as a ferromagnetic, metal-like band-conductor and above T_C as a paramagnetic semiconductor, displaying a huge, magnetic order-related resistivity peak near 200 K. Weakly structured MAEs, occurring in the temperature range 4 K $< T <$ 190 K with logarithmic time dependence, are attributed to continuously superimposed Debye processes with activation enthalpy spectra in the range $0.008 < Q < 0.5$ eV and pre-exponential factors, τ_0, of 10^{-12} to 10^{-11}s. These enthalpy spectra are related to electrons which, due to localization at Jahn–Teller stabilized Mn^{3+}-ions, are able to contribute to MAEs only after thermal activation. According to our analysis, charge transport in the semiconducting phase, above T_C, is supported by hopping of small polarons with activation enthalpies, Q, of about 0.15 eV.

1. Introduction

The magneto-electronic properties of alkaline- (A-) doped rare earth (R) perovskites of the general composition $R_{1-x}A_xMnO_3$ (R $\hat{=}$ La, Nd, Pr; A $\hat{=}$ Ca, Sr, Ba) can be varied, in dependence of the doping rate x, within a wide range extending from an antiferromagnetic insulator ($x = 0$) over a ferromagnetic conductor ($0.2 \leqslant x \leqslant 0.5$) to an anti-ferromagnetic semiconductor ($x = 1$) [1, 2]. The profound interest in the relation between conductivity and such versatile material behaviour [3–7] became further stimulated by the recent discovery of a giant (GMR), or even colossal (CMR), magnetoresistance in these materials [8, 9]. This spectacular anomaly of the electric conductivity was found to arise in moderately doped compounds during the transition from the low-temperature ferromagnetic, metal-like conducting phase into the paramagnetic, semiconducting state above the Curie temperature, T_C [8–13]. Despite the enormous efforts undertaken in recent years it has not been possible, as yet, to obtain full insight into the driving mechanisms producing the observed CMRs. On the other hand it became clear, however, that these extraordinary effects owe their existence to a subtle interplay between order-dependent charge carrier transport, magnetic order and crystallographic structure [8–13], the latter being eventually affected, moreover, by specific Jahn–Teller induced distortions [14–17]. Recently the occurrence of such CMR peaks near the Curie temperature has been associated with an interrelation between magnetic and polaronic order [18]. According to this model in the low-temperature phase ($<T_C$), on account of strong magneto-polaronic exchange interactions, only single-state polarons can exist which, by means of incoherent tunnelling, are responsible for the relatively high conductivity of the material. Above T_C, however, in the absence of these interactions, the polarons are expected to coalesce to immobile bipolarons, capable of charge transport only after thermal dissociation, by means of hopping.

0953-8984/99/458901+12$30.00

In this situation it appears promising to extend the investigations on this class of materials by the application of magnetic after-effect (MAE) spectroscopy—a technique which, previously, allowed us to contribute appreciably to the elucidation of the conductivity mechanisms in the related inverse-spinel structured magnetite (Fe_3O_4) and its derivatives [19–23]. This was enabled by the high sensitivity of the MAE technique to time- and/or temperature-dependent susceptibility variations, which, in the ionically ordered ferro- or ferrimagnetic phase of nonmetallic compounds, like the rare-earth type perovskites discussed here, or the previous magnetite-based ferrites, are intimately related to corresponding charge carrier transport mechanisms. Due to these magneto-electronic interrelations, valuable information concerning electric conduction mechanisms may be obtained from the analysis of corresponding magnetic relaxation spectra [22–26].

Thus, our present report is intended to demonstrate to what extent MAE investigations may contribute to an understanding of the magneto-electronic properties of ionically ordered ferromagnetic perovskites, like polycrystalline $La_{0.8}Ca_{0.2}MnO_3$. The results obtained on this compound may be regarded as representative for a series of related, similarly studied systems such as $La_{1/3}Nd_{1/3}Ca_{1/3}MnO_3$ [24] or $Sm_{0.7}Sr_{0.3}MnO_3$, $La_{0.66}Ca_{0.33}MnO_3$ and $La_{0.3}Sr_{0.3}Pb_{0.4}MnO_3$ (unpublished results).

2. Experimental techniques

2.1. Specimen preparation

Polycrystalline specimens were prepared from mixtures of La_2O_3, MnO_3 and CaO. These mixtures were pressed into pellets and prefired at 1100 °C in air for 24 h. The obtained products were ball-milled to powder, of which rods were isostatically pressed (2500 bar) and sintered at 1350 °C in oxygen for 24 h, followed by furnace cooling. The final product was proved by x-ray and SEM to be *crystallographically* single-phase material. Microscopic inspection indicated that the average grain size is of the order of 10 μm.

The x-ray diffraction pattern could be indexed in a first approximation by a cubic structure with a lattice parameter of 7.766 Å, which means a doubling of the single perovskite lattice in three dimensions. However, the line-broadening and fine structure of the diffraction lines suggest the real structure, instead of being cubic, to be rather orthorhombic, with the axes $a = 5.472$ Å, $b = 5.512$ Å and $c = 7.663$ Å.

Chemical analysis of the sintered material revealed a Mn^{4+} concentration of 0.24 per formula unit, thus pointing to a slight oxidation of the specimens: $La_{0.8}Ca_{0.2}MnO_{3.02}$.

The final polycrystals were wire-sawn (spark-erosion failed because of the low room-temperature conductivity) into prismatic rods of 1.4 mm × 1.4 mm × $\leqslant$20 mm.

2.2. Magnetic after-effect measurements

MAE measurements were performed within the temperature range 4.4 K $\leqslant T <$ 500 K, by means of a sensitive automated LC-oscillator technique, working in the 1 kHz range [24]. The time dependence of the reciprocal susceptibility (χ), i.e. the reluctivity $r(t, T) = 1/\chi(t, T)$, was recorded, departing from exactly 1 s (t_1) after a well defined sample demagnetization, over the time interval of 2 s $\leqslant t_2 \leqslant$ 180 s. Making use of the real-part susceptibility components, as measured between t_1 and the range of ensuing times t_2, the isochronal relaxation spectrum is constructed in the following way:

$$\frac{\Delta r}{r_1} = \frac{\Delta r(t_1, t_2, T)}{r(t_1, T)} = \frac{r(t_2, T) - r(t_1, T)}{r(t_1, T)}. \tag{1}$$

This data presentation has the advantage of clearly resolving individual contributions of superimposed multi-process relaxations, e.g. in the form of separated peaks, within the wide MAE spectrum extending over the whole temperature range investigated [26].

3. Experimental results

3.1. Temperature dependence and hysteresis of magnetic parameters

Figure 1 shows (a) the MAE spectrum of polycrystalline $La_{0.8}Ca_{0.2}MnO_3$ and (b) the corresponding initial susceptibility as obtained when measuring in the heating mode, i.e. by progressing from a temperature of about 4.4 K—attained by rapidly cooling down ($\sim$1 K s^{-1}) the crystal from room temperature—up to Curie temperature of about $T_C \simeq 190$ K. The dashed lines in these figures represent the MAE amplitude ($t_2 = 180$ s) and the susceptibility as observed during the reversed measuring mode, i.e. during stepwise cooling down from temperatures above T_C. Irrespective of these measuring modes (heating or cooling), identical temperature dependencies of $\Delta r/r_1$ and χ_0 are found in the temperature range 90 K $< T <$ 220 K, whereas in the lower regime, 4 K $< T <$ 90 K, these respective effects appear with reduced strength when measured in the cooling as compared to the heating mode. This irreversibility of relaxation amplitudes with respect to the sense of temperature variation is resolved into a larger scale in figures 2(a) and (b) and thoroughly discussed in section 4. Both the pronounced susceptibility decay at T_C and the accompanying strong magneto-resistive effect, culminating in a huge resistivity maximum near 200 K (cf figure 4), point to the fact that below T_C our material may be characterized as a ferromagnet. Inset into figure 1(a) is the MAE spectrum of single-crystalline, stoichiometric magnetite (Fe_3O_4) in order to allow comparison between the related, electronically induced low-temperature relaxations occurring in both systems (cf section 3.2).

3.2. Time dependence of the magnetic relaxation

Typically, the MAE spectra of our investigated perovskites are characterized by only softly amplitude-modulated relaxation regimes extending over relatively wide temperature ranges—bare of any discrete, thermally activated Debye-type peak. As shown in figure 3, the magnetic relaxation follows with high accuracy, over the full temperature range of 4 K $< T <$ 220 K, a logarithmic time dependence of the type

$$r(t) = A + B \ln t. \tag{2}$$

Such a dependence is characteristic for the superposition of a continuum of Debye processes with their relaxation times, τ_1, being steadily distributed over the range $\tau_1 \leqslant \tau_i \leqslant \tau_2$, and with measuring times, t_i, obeying the conditions $\tau_1 \ll t_i \ll \tau_2$ [26, 27]. This can be deduced from the corresponding relaxation function

$$G(t) = 1 + \frac{1}{\ln \tau_2/\tau_1}\{\mathrm{Ei}(-t/\tau_2) - \mathrm{Ei}(-t/\tau_1)\} \tag{3}$$

being expressed in terms of the Arrhenius-type relaxation times:

$$\tau_i = \tau_0 \, \mathrm{e}^{Q/kT} \tag{4}$$

and the so-called exponential integrals [26, 27]:

$$\mathrm{Ei}(-t/\tau_i) = -\int_{t/\tau_i}^{\infty} \frac{\mathrm{e}^{-t/\tau_i}}{t/\tau_i} \, \mathrm{d}(t/\tau_i). \tag{5}$$

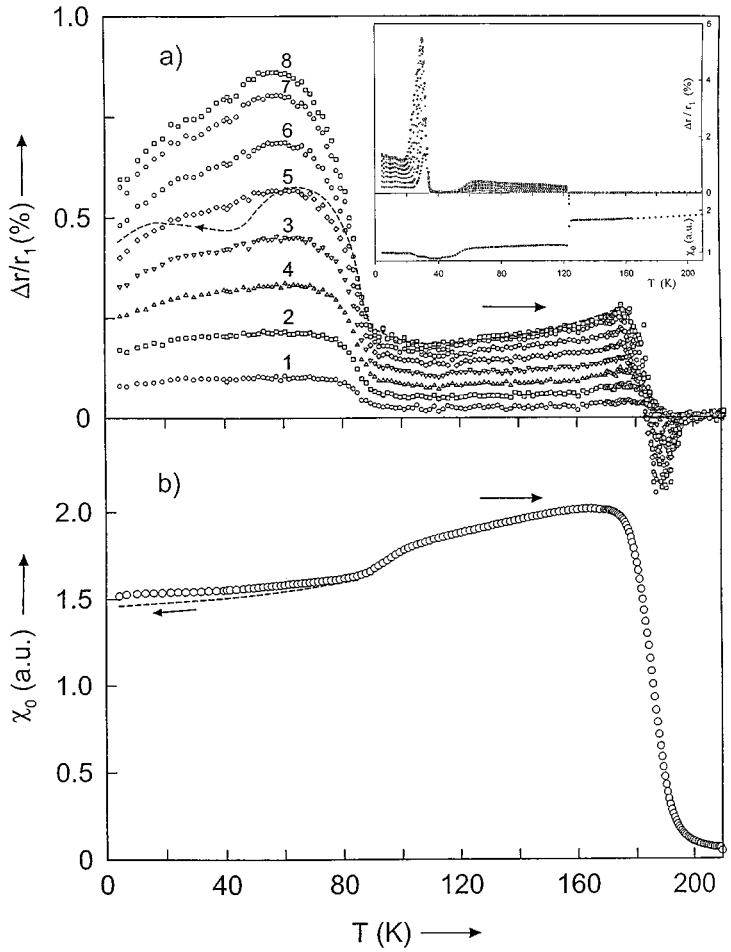

Figure 1. (a) MAE spectrum of $La_{0.8}Ca_{0.2}MnO_3$ extending over the ferromagnetic phase of the material (4 K $< T <$ 200 K). The time parameters, t_2, of the isochronals (cf section 2.2) are given by their numbering as follows: $t_1 = 1$ s and $t_2 = 2$ s (1), 4 s (2), 8 s (3), 16 s (4), 32 s (5), 64 s (6), 128 s (7) and 180 s (8). The arrows visualize the applied measuring mode, i.e. (i) heating (family of isochronals) or (ii) cooling (dashed isochronal, corresponding to $t_2 = 180$ s).

The inset shows the related MAE spectrum of single-crystalline, stoichiometric magnetite (Fe_3O_4) within the same temperature range. Typically, this spectrum, too, is composed of two *electron-induced*, plateau-like relaxation zones of *logarithmic time-dependence*, resulting from (i) tunnelling (4 K $< T <$ 25 K) and (ii) hopping (50 K $< T <$ 125 K); in addition, near 30 K, discrete Debye processes, induced by *intra-atomic* excitations of electrons, are observed [22]. (b) Initial susceptibility, as obtained during the measuring runs of figure 1(a), heating and cooling (dashed line) being indicated by respective arrows.

Being aware of the above noted limitations for the relaxation times τ_i, the exponential integrals in (3) can be developed into rapidly converging series which, by appropriate summing up, yield the following approximation, with $C = 0.5772$ the Euler constant [26]:

$$G(t) \simeq 1 + \frac{1}{\ln \tau_2/\tau_1}\left(C + \ln \frac{t}{\tau_2}\right). \tag{6}$$

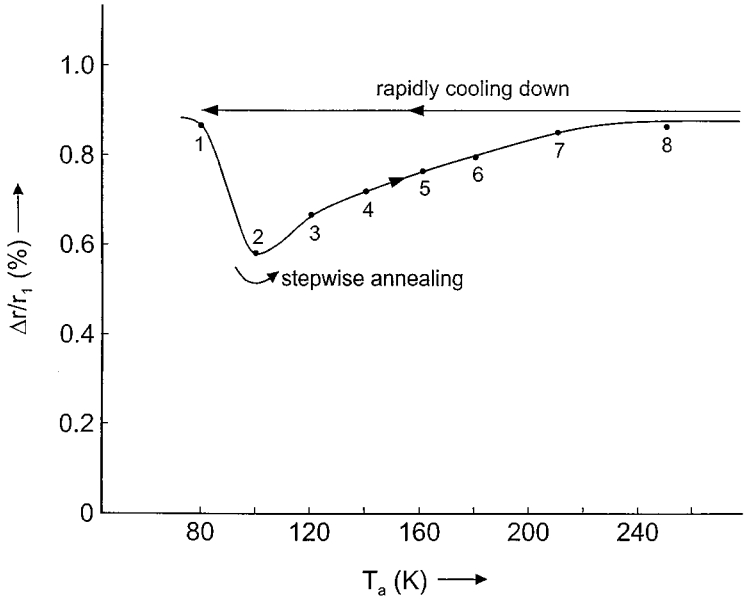

(a)

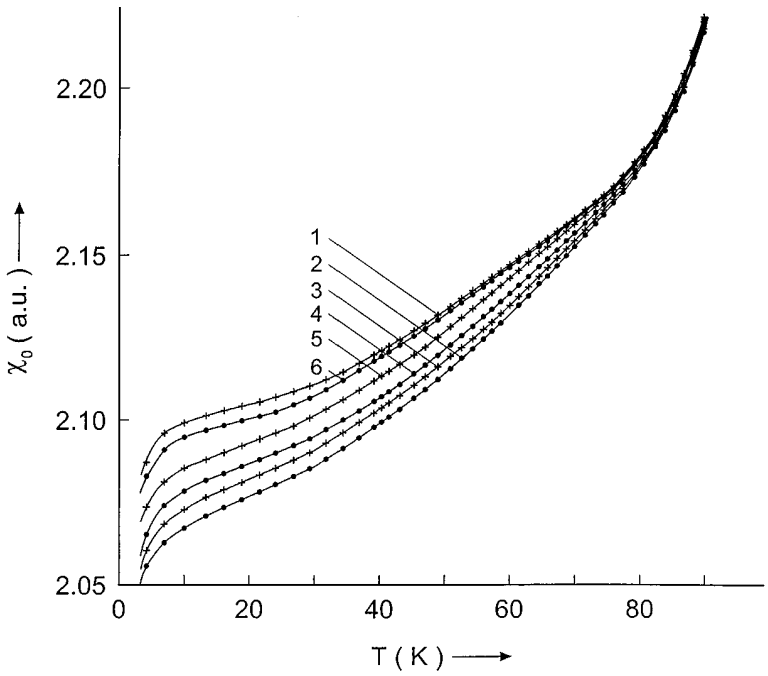

(b)

Figure 2. (a) High-scale resolution of the recovery of the irreversibly frozen-in relaxation strength, as determined at $T = 60$ K over the time interval $t_1 = 1$ s, $t_2 = 180$ s. As starting condition for these measurements the crystal was *rapidly cooled down* to 4.4 K (1); the numbered points (2)–(8) represent the MAE amplitudes as obtained after subsequent annealing to the indicated temperatures, *slowly cooling down again* to 4.4 K and remeasuring the resulting relaxation at $T = 60$ K. (b) Recovery of the initial susceptibility, as observed between 4.4 K and the critical temperature ($T \approx 90$ K) during the measuring runs described in (a).

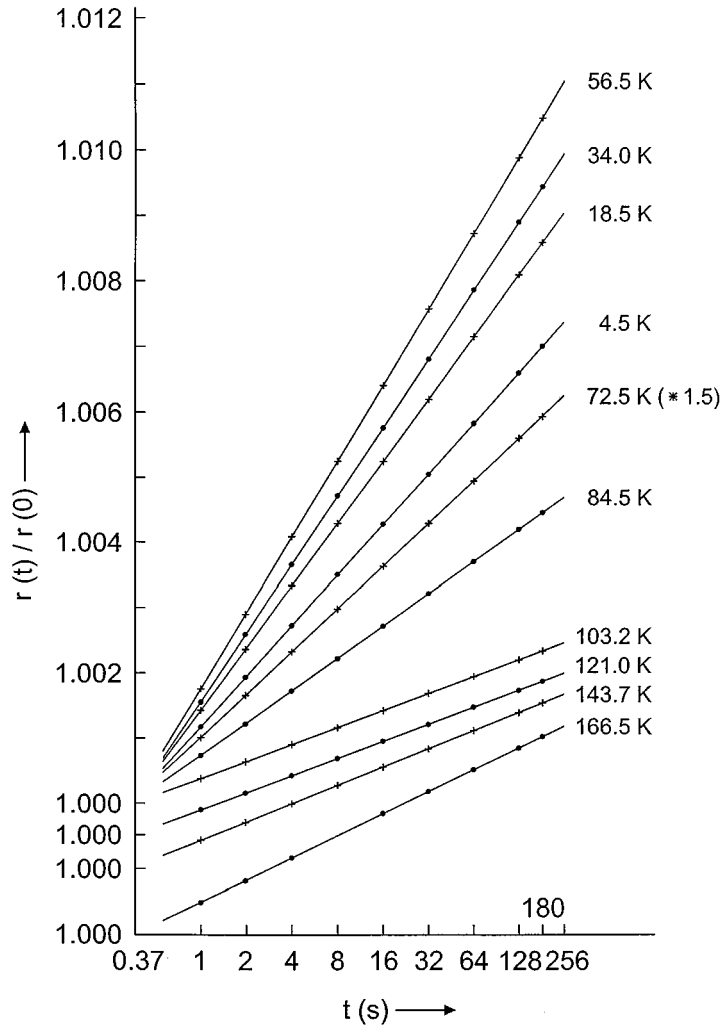

Figure 3. Representative analysis concerning the time dependence of various isothermals composing the MAE spectrum—yielding with high accuracy, over the whole temperature range investigated, logarithmic dependency. The numbers characterizing the straight lines are the Kelvin temperatures of the respective isothermals. In order to obtain concise data presentation, the amplitudes of the 72.5 K isothermal had to be reduced; they can be reproduced by multiplying the given data by a factor of 1.5.

Insertion of equation (6) into the general isothermal, time-dependent reluctivity relation evolving after sample demagnetization:

$$r(t) = r(0) + \Delta r_s \, G(t) \tag{7}$$

(with $r(0)$ and Δr_s denoting, respectively, the initial reluctivity at time $t = 0$ and the stabilization reluctivity, i.e. the difference $r(t_2) - r(0)$ in the limit $t_2 \to \infty$) results, indeed in the logarithmic time dependence of equation (2), which is checked in figure 3 and found to be appropriate over the whole temperature range.

By assuming the pre-exponential factors τ_{0i} here to be of the same order of magnitude—$10^{-12} < \tau_{0i} < 10^{-11}$ s—as in the related case of logarithmic low-temperature relaxations in

magnetite (cf inset of figure 1(a), [22]), we can estimate the corresponding enthalpy spectrum within the basic temperature range 4 K $< T <$ 90 K to $0.008 \leqslant Q \leqslant 0.3$ eV. By extending this model also to the higher-temperature logarithmic relaxation regime, 90 K $< T <$ 190 K, the upper limit of the enthalpy spectrum amounts to $Q \lesssim 0.5$ eV.

3.3. Transition-modulated structure of the MAE spectra

On inspection of figure 1, we recognize a considerable drop of the relaxation strength near 80 K, being accompanied at its upper end, at about 90 K, by a spontaneous increase of the susceptibility. These variations indicate a specific type of intrinsic phase transition (cf section 4) due to—possibly combined—electronic and/or crystalline reordering, thus leading to both an increased domain-wall mobility and enhanced charge transport, the latter causing reduced relaxation strength. It is most interesting that, depending on the chosen heating mode, we observe characteristic hysteresis effects only below this transition temperature, as shown in figure 2 for the relaxation strength (a) and the susceptibility (b), cf section 3.1. The transition from the ferromagnetic into the paramagnetic state is indicated near 190 K, i.e. the Curie temperature, by the concomitant decay of the magnetic relaxation and the susceptibility, figure 1.

3.4. Temperature dependence of the electric resistivity

Figure 4 shows the relatively strong temperature dependence of the magnetic order-related resistivity in our material, as obtained on a prismatic rod of 1.4 mm × 1.4 mm × 9 mm. Analysis of these data, as described below, yields a specific resistivity of about $\leqslant 10^{-1}$ Ω cm at both the low-temperature (4.4 K) and high-temperature (300 K) end of the pronounced maximum situated near $T_M \simeq 200$ K, slightly above the Curie temperature ($T_C \simeq 190$ K), cf figure 4. This maximum is indicative for the intrinsic, magnetic-order-dependent conductivity mechanisms controlling our present and related perovskites, pointing, on first inspection, to metal-like band conductivity in the ferromagnetic phase below T_M and to semiconductivity in the paramagnetic phase above T_M, cf section 4.1. Numerical evaluation of the high-temperature slope of this resistivity curve, $\rho(T)$, in terms of intrinsic semiconductivity [28, 29]:

$$\rho(T) = \{n(T)\mu e\}^{-1} \tag{8}$$

(n, μ and e denoting, respectively, the number of charge carriers, electrons and holes, the carrier mobility and the electron charge), yields, by assuming the typical temperature dependency of $n(T)$ [28, 29], against which the one of $\mu(T)$ may be neglected:

$$n(T) = 2(\pi kT/h^2)^{3/2} M^* \exp(-E_g/2kT) = AT^{3/2} \exp(-E_g/2kT) \tag{9}$$

(k is the Boltzmann and h the Planck constant and M^* the effective carrier mass [29]), a value of $E_g \simeq 0.15$ eV for the energy gap between the valency and conductivity bands of the semiconductor, cf section 4.1. The dashed curve in figure 4 is obtained by extrapolation of the corresponding semiconducting state down to temperatures below T_M (T_C), thereby using the parameters as deduced from the described resistivity analysis.

4. Discussion

4.1. Magnetic relaxation mechanisms

$LaMnO_3$, originally an insulating antiferromagnet in the temperature range below the Néel temperature, $T_N \simeq 160$ K [10], changes its character completely into a metal-like conducting

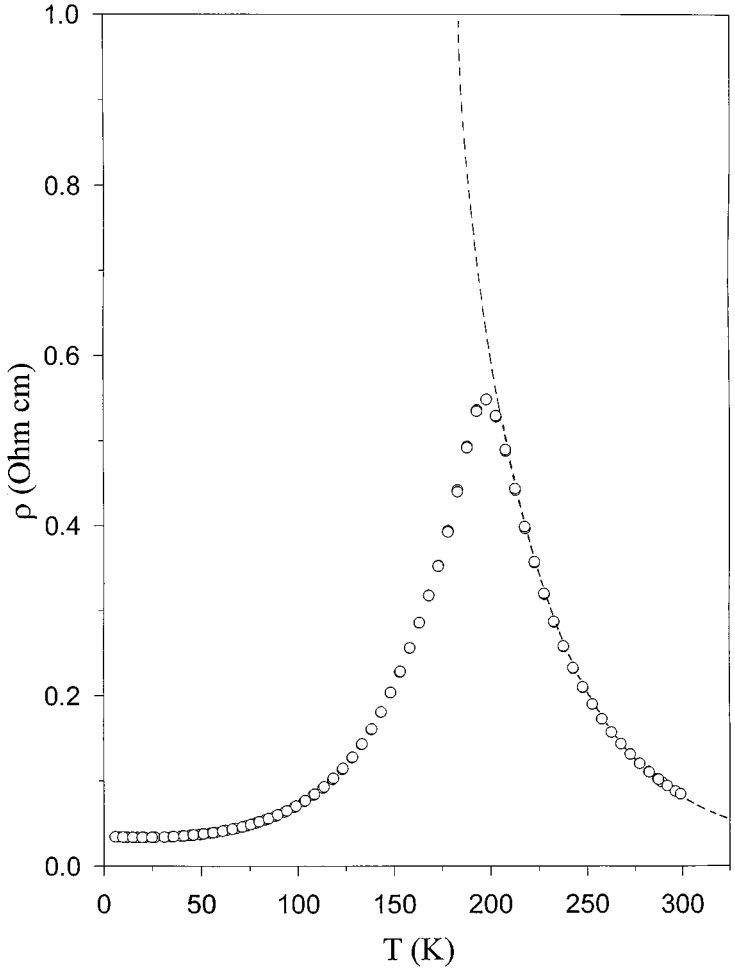

Figure 4. Temperature dependence of the magnetic order-related resistivity in $La_{0.8}Ca_{0.2}MnO_3$, displaying a pronounced maximum at 200 K. The variation in the high-temperature range ($T > 200$ K) corresponds to that of an intrinsic semiconductor, as indicated by the dashed line. This has been constructed using the data of a numerical analysis yielding an activation enthalpy of $Q = 0.15$ eV (cf section 3.4). The low-temperature ($T < 200$ K) dependency, on the other hand, resembles that of a metallic conductor. The resistivity has been determined using a high-precision four-point measuring technique with a current of 1 mA.

ferromagnet, with Curie temperatures in the range 180 K $< T_C <$ 280 K [10], by doping with appropriate amounts x of a bivalent alkaline earth, like Ca, i.e. $0.2 \leqslant x \leqslant 0.8$. As pointed out in sections 1 and 3 our currently investigated material is exactly of this latter type. This dramatic alteration of intrinsic properties is a consequence of the Ca^{2+} substitution which, in order to maintain charge neutrality, causes a corresponding amount of Mn^{3+} ions to change their valency into Mn^{4+}. Pairs of such differently valent Mn ions, placed along an edge of the perovskite lattice, are able to interact with each other via double exchange electron hopping over the p orbitals of an intermediately situated O^{2-} ion, cf figure 5, according to the following scheme

$$Mn_1^{3+}\text{—}\,O^{2-}\text{—}\,Mn_2^{4+} \leftrightarrows Mn_1^{4+}\text{—}\,O^{2-}\text{—}\,Mn_2^{3+}.$$

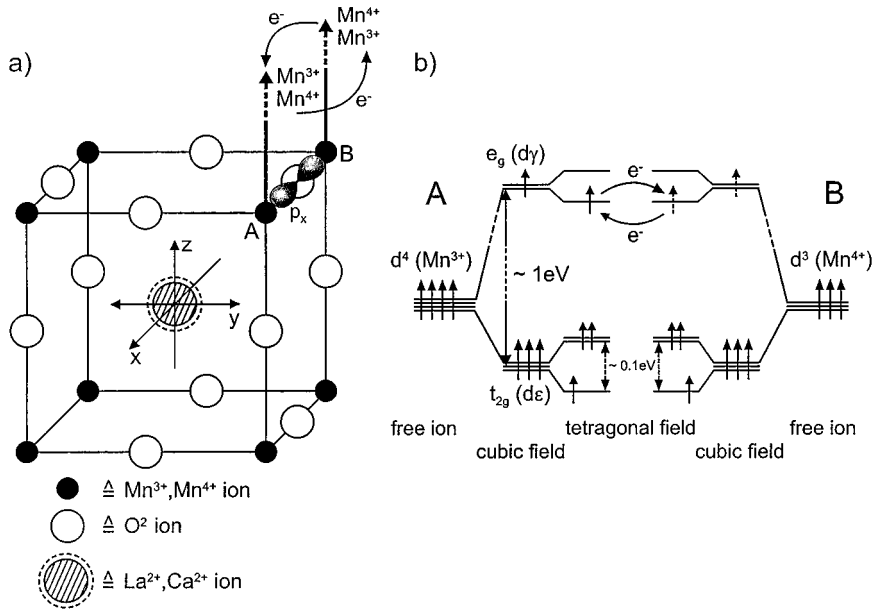

Figure 5. (a) Model of the $La_{0.8}Ca_{0.2}MnO_3$ perovskite lattice, illustrating the mechanism of double exchange via p electrons of an oxygen ion residing between two Mn ions A and B. (b) Level diagrams of Mn^{3+} and Mn^{4+} ions, explaining in more detail the electron transfer between the corresponding ions A and B of (a) in terms of an exchange of e_g electrons.

Evidently, this mechanism is able to support both enhanced conductivity—via facilitated electron transfer between neighbouring Mn sites—and, in addition, enhanced magnetic order since, upon exchange, the hopping electrons preserve their original spin orientation thereby contributing, in agreement with Hund's rules, to the magnetic moments of their host ions [3, 4, 32, 33]. This combined local transfer of electronic charge and magnetic moment, due to interactions with the spontaneous domain wall anisotropy, leads to a decrease of the total crystal energy, thereby giving rise to magnetic relaxations.

4.2. Band to semiconductor transition

The maximum in the temperature dependence of the specific resistivity $\rho(T)$, at $T_M \simeq 200$ K—situated only slightly above the Curie temperature $T_C \simeq 190$ K of the compound—separates clearly two regimes of different charge transport, cf figure 4. Above T_M the resistivity, by its sharp increase to lower temperatures, indicates semiconducting behaviour, cf section 3.4, whereas below T_M its character resembles that of a band-conducting metal†. Typically, this band conduction is limited to the ferromagnetic state within which only—due to the magnetic order—enhanced electron transfer is activated in the form of double exchange. With the breakdown of the ferromagnetic order, at temperatures $T \geqslant T_C$, this mode of enhanced electron transfer is destroyed and the conductivity mechanism thrown back to thermally activated carrier

† It seems worthwhile, however, to point to the fact that the classification of perovskites as metallic conductors below and semiconductors above T_M is justified only with respect to the *temperature coefficients* of the resistivity within these two temperature regimes. The absolute resistivity values of our material at $T \geqslant 4$ K and $T \simeq 300$ K differ only by a factor of about 2 being, however, about a factor of $>10^4$ larger than the room-temperature data of a well conducting metal like copper ($\rho \simeq 1.7 \times 10^{-6}$ Ω cm) and still about a factor of $\leqslant 10$ above that of magnetite ($\rho \simeq 10^{-2}$ Ω cm at RT [32]).

transport, cf section 4.3. This conductivity behaviour may be described in terms of a phonon-induced narrowing and final destruction of the conduction band upon approaching the Curie temperature T_C above which, consequently, conductivity remains limited to thermally activated hopping of small polarons.

It is interesting to note that in terms of the polaron–bipolaron model [18], mentioned in section 1, the high-temperature activation enthalpy (E_g) above T_C should be identified, essentially, with the binding energy of bipolarons. Indeed, we find our result for E_g (0.15 eV, cf section 3.4) to compare well with corresponding literature data obtained on related compounds, such as WO_{3-x} [30] and La_2CuO_4 [31].

4.3. Electron localization and magnetic after-effects

The observation of MAEs with logarithmic time dependency in the ferromagnetic phase below T_C—being interpretable as continuous superpositions of thermally activated processes, cf section 3.2—points to a localization of electrons already in the band-conducting state. It may be useful here to remember that, in our present materials, at a given temperature only those processes can be observed by the MAE whose relaxation times, according to equation (4), are of the order of the observation times (1 s $< \tau <$ 180 s). Processes with, especially, shorter time constants fall outside the range of MAE observation. In this way only a (possibly smaller) part of all conductivity-contributing carriers can be detected by means of the MAE. This is supposed to be also the reason why the pronounced drop of the relaxation strength, together with the corresponding rise of the susceptibility, near 90 K (figures 1(a), (b)) is not reflected by the electric resistivity (figures 2, 4). Thus, in terms of our model, the observed MAEs are attributed to electrons (polarons) which, even in the low-temperature state of 'metallic conductivity', are localized and only after thermal activation contribute to the conductivity, according to equation (9). The origin of this localization is seen in Mn^{3+}-induced local Jahn–Teller (JT) lattice distortions by which the free electron exchange between differently valent Mn ions (equation (9)) is interrupted in favour of a stabilization of the ionic Mn^{3+} and Mn^{4+} states. The order of magnitudes of these presumably JT-induced localization enthalpies, which have to be overcome by thermal activation in order to enable charge transfer in combination with magnetic relaxation, compare well with the similarly Fe^{2+}- anisotropy-induced activation enthalpies of electron hopping in magnetite, i.e. 0.1 eV $< Q <$ 0.35 eV within the temperature range of 35 K $< T <$ 125 K [22]. They are also in agreement with the Mn^{3+}–JT-induced extra enthalpies of vacancy migration in Mn-doped magnetites, reaching up to $Q \geqslant 0.5$ eV [34].

4.4. Reversible and irreversible transitions below T_C

The rapid decay of the magnetic relaxation strength near 90 K in the MAE spectrum, being accompanied by a corresponding increase of the susceptibility (figures 1(a), (b)), points to a combined transition of the crystallographic and magnetic order. Since, evidently, during this transition the domain wall mobility becomes increased, we assign it to a structural transformation from lower to higher (cubic) crystallographic order being achieved, e.g. by a release of Mn^{3+}-based, JT-induced lattice distortions. Thus, the irreversibility of the 90 K transition, with respect to the cooling rate across the conversion point (cf figure 1, section 3.1), may be attributed to an enforced freezing in of lattice distortions due to cooperative JT effects becoming especially active during the slower cooling rate. In this latter case, therefore, the imposed stresses recover only during the subsequent annealing of the crystal up to room temperature, as reflected by the related recovery of the relaxation strength and the susceptibility (figures 2(a), (b)).

An additional mechanism supporting the decay of the MAE amplitude near 90 K could be seen also in a magnetic phase separation into minor antiferromagnetic inclusions embedded within the predominating ferromagnetic matrix of our $La_{0.8}Ca_{0.2}MnO_3$ polycrystals [35–37]. According to Troyanchuk *et al* [35, 36] it is feasible for such inclusions to occur within the concentration range ($x \leqslant 0.2$) of our specimens. With the disappearance of such antiferromagnetic inclusions, upon their transition into the paramagnetic phase (near 90 K), obstacles to domain-wall mobility and accelerated long-range electron exchange would become eliminated, thus causing a reduction of the observable relaxation strength (cf section 4.2, figure 1(a)) in combination with an increase of the initial susceptibility (figure 1(b)). In addition, it is feasible, as well, for the envisaged antiferro- to paramagnetic phase transition to be accompanied by a release of lattice distortions—regarded as possible sources for the observed hysteresis effects—and thus it could also contribute to the irreversible MAE and susceptibility behaviour of the material (cf figures 1, 2).

5. Summary

(i) MAE and electric resistivity measurements prove—i.e. by a strong susceptibility drop at a relatively high Curie temperature (190 K) and a pronounced resistivity peak (200 K)—that our polycrystalline $La_{0.8}Ca_{0.2}MnO_3$ compound, below T_C, is a well ordered ferromagnetic, metal-like band conductor which, above T_C, changes into a paramagnetic semiconductor.

(ii) The measured logarithmic time dependence of the magnetic relaxations—extending over the temperature range 4 K $< T <$ 200 K—is associated with a continuous superposition of Debye processes, resulting from a correspondingly wide enthalpy distribution ($0.008 < Q < 0.5$ eV). This energy spectrum is attributed to Jahn–Teller (JT) stabilized electrons which, only after thermal activation, are able to participate in the combined electronic charge and magnetic anisotropy transfer giving rise to the observed MAEs.

(iii) A structural transition near 90 K—giving rise, upon heating up, to a spontaneous decay of the relaxation strength and an increase of the susceptibility—is related to a release of JT-induced internal stresses; additionally, these effects are discussed in terms of an antiferro- to paramagnetic phase transition of a possibly included residual, antiferromagnetic, second phase. In terms of the JT model, upon slowly cooling down below this transition point, enhanced cooperative extra JT distortions are frozen in, thus producing temperature-dependent parameter irreversibilities which can be completely eliminated only after annealing the specimen up to about 300 K.

(iv) Upon approaching the Curie temperature, due to enhanced phonon interactions, the conduction band of the low-temperature phase becomes narrowed down and finally eliminated, thereby transforming the material into a semiconductor whose residual charge transport is accomplished by small polaron hopping, for which an activation enthalpy of 0.15 eV has been determined.

Acknowledgments

The authors are very grateful to Dr V A M Brabers for providing the well defined $La_{0.8}Ca_{0.2}MnO_3$ polycrystals, as well as for many helpful and stimulating discussions. They further express their thanks to Mrs G Siegle for performing instructive resistivity measurements and to Mrs A Weisshardt and Th Dragon for conducting valuable SEM analyses on the material.

References

[1] Jonker G H and van Santen J H 1950 *Physica* **16** 337
Jonker G H and van Santen J H 1953 *Physica* **19** 120
[2] Wollan E O and Koehler W C 1955 *Phys. Rev.* **100** 545
[3] Zener C 1951 *Phys. Rev.* **82** 403
[4] Anderson F W and Hasegawa H 1955 *Phys. Rev.* **100** 675
[5] Goodenough J B 1955 *Phys. Rev.* **100** 564
[6] de Gennes P G 1960 *Phys. Rev.* **118** 141
[7] Kusters R M, Singleton J, Keen D A, McGreevy R and Hayes W 1989 *Physica* B **155** 362
[8] Chahara K, Ohno T, Kasai M and Kozono Y 1993 *Appl. Phys. Lett.* **63** 1990
[9] Jin S, Tiefel T H, McCormac M, Fastnacht R A, Ramesh R and Chen L H 1994 *Science* **264** 413
[10] Schiffer P, Ramirez A P, Bao W and Cheong S W 1995 *Phys. Rev. Lett.* **75** 3336
[11] Radaelli P G, Cox D E, Marezio M, Cheong S W, Schiffer P E and Ramirez A P 1995 *Phys. Rev. Lett.* **75** 4488
[12] Rao G H, Sun J R, Liang J K and Zou W Y 1997 *Phys. Rev.* B **55** 3742
[13] Uhlenbruck S *et al* 1999 *Phys. Rev. Lett.* **82** 185
[14] Inoue J and Maekawa S 1995 *Phys. Rev. Lett.* **74** 3407
[15] Hwang H Y, Cheong S W, Radaelli P G, Marezio M and Batlogg B 1995 *Phys. Rev. Lett.* **75** 914
[16] Millis A J, Shraiman B I and Mueller R 1996 *Phys. Rev. Lett.* **77** 175
[17] Kawano H, Kajimoto R, Yoshizawa H, Tomioka Y, Kuwahara H and Tokura Y 1997 *Phys. Rev. Lett.* **78** 4253
[18] Alexandrov A S and Bratkovsky A M 1999 *J. Phys.: Condens. Matter* **11** 1989
[19] Kronmüller H, Schützenauer R and Walz F 1974 *Phys. Status Solidi* a **24** 487
[20] Kronmüller H and Walz F 1980 *Phil. Mag.* B **42** 433
[21] Walz F, Brabers V A M, Chikazumi S, Kronmüller H and Rigo M O 1982 *Phys. Status Solidi* b **110** 471
[22] Walz F and Kronmüller H 1990 *Phys. Status Solidi* b **160** 661
Walz F and Kronmüller H 1994 *Phys. Status Solidi* b **181** 485
[23] Walz F and Brabers V A M 1996 *Phys. Status Solidi* a **156** 471
Walz F and Brabers V A M 1998 *Phys. Status Solidi* a **168** 281
[24] Baszynski J, Walz F and Tolinski T *Proc. 2nd Eur. Conf. on Magnetic Sensors and Actuators (Sheffield, 1998)* at press
[25] Walz F 1971 *Phys. Status Solidi* a **8** 125
Walz F 1974 *Appl. Phys.* **3** 313
Walz F 1984 *Phys. Status Solidi* a **82** 179
Walz F 1995 *Phys. Status Solidi* a **147** 237
[26] Kronmüller H 1968 *Nachwirkung in Ferromagnetika* (Berlin: Springer)
[27] Kneller E 1962 *Ferromagnetismus* (Berlin: Springer)
[28] Finkelnburg W 1958 *Einführung in die Atomphysik, 6 Auflage* (Berlin: Springer)
[29] Decker A J 1981 *Solid State Physics* (London: MacMillan)
[30] Salje E K H 1995 *Polarons and Bipolarons in High-T_C Superconductors and Related Materials* ed E K H Salje, A S Alexandrov and W Liang (Cambridge: Cambridge University Press) p 116
[31] Alexandrov A S and Mott N 1995 *Polarons and Bipolarons* (Singapore: World Scientific) p 37f
[32] Smit J and Wijn H P J 1959 *Ferrite* (Eindhoven: Philips)
[33] Krupicka S 1973 *Physik der Ferrite* (Braunschweig: Vieweg)
[34] Walz F and Rivas J 1976 *Phys. Status Solidi* a **37** 151
Walz F, Rivas J, Brabers J H V J and Kronmüller H 1999 *Phys. Status Solidi* a **173** 467
[35] Troyanchuk I O, Bychkov G L and Bogush A K 1989 *Sov. Phys.–Solid State* **31** 1445
[36] *Landolt–Börnstein New Series* 1996 Group III, vol 27- F.1α ed H P J Wijn (Berlin: Springer) p 152
[37] Moreo A, Yunoki S and Dagotto E 1999 *Science* **283** 2034